Rare Metal Materials and Engineering
Volume 49, Issue 2, February 2020
Available online at www.rmme.ac.cn

Science Press

Cite this article as: Rare Metal Materials and Engineering, 2020, 49(2): 0412-0421.

ARTICLE

Corrosion Behavior of Carbon Steel and Iron-Chromium-Nickel Alloys in Molten Eutectic Sodium Chloride and Magnesium Chloride as Phase Change Materials

Wang Junwei[1,2], Bao Zelong[1], Ye Haihua[1], Ma Qing[3], Jia Hongguang[1,2]

[1] The College of Mechanical Engineering, Qinghai University, Xining 810016, China; [2] Qinghai Provincial Key Laboratory of New Light Alloys, Qinghai University, Xining 810016, China; [3] State Key Laboratory of Plateau Ecology and Agriculture, Qinghai University, Xining 810016, China

Abstract: As a phase change material for solar energy storage at moderate-high temperatures, the molten eutectic chloride salt of sodium chloride and magnesium chloride (NaCl-52 wt% $MgCl_2$) is strongly corrosive to metal containers and pipes. The corrosion behavior of three kinds of iron-chromium-nickel (Fe-Cr-Ni) alloys and carbon steels in the molten eutectic salt at 520 °C was studied. Results show that the carbon steel is corroded along grain boundaries, and iron atoms become ferrous ions (Fe^{2+}) and ferric ions (Fe^{3+}). A thick and compact magnesium oxide (MgO) shell is formed on the surface of carbon steel, which protects the specimen from corrosion. The MgO shell is also formed on the surface of three kinds of iron-chromium-nickel alloys, but the magnesium oxide shell cannot protect them from corrosion in the molten salt. A loose skeletal Ni-rich microstructure is formed on the specimen surface because the chromium element is preferentially corroded. The magnesium oxide (MgO) shell or particles peel off easily. In addition, the higher the content of the chromium, the more severe the corrosion. As a vessel or pipe material for solar energy storage by molten chloride salt, cheap iron-based alloys with alloying element nickel have greater development prospects.

Key words: molten chloride salt; high temperature corrosion; magnesium oxide; stainless steel; carbon steel

At present, fossil energy is facing exhaustion. And the environmental pollution is very serious. Solar energy is one of the new renewable energy sources, which will probably replace the fossil energy[1,2]. The utilization form of the solar energy includes the photo-voltaic, photo-thermal, photo-chemistry and photo-biology[3-6]. There are still many technical problems about solar energy storage and conversion[2,5,7-9]. The utilization field of the photo-thermal has been extended to the solar power, solar heating, solar steam drying, etc[1,10,11]. However, solar energy is discontinuous for the influence of night, dust and clouds, which will decrease the solar energy photo-thermal system efficiency.

In order to improve the thermal efficiency, using molten salt as a phase change material (PCM) to store solar energy at moderate-high temperatures is a good way[12,13]. PCM stores thermal energy when it melts, and releases energy when it solidifies. Consequentially, it is very important to match the melting temperature of the PCM to the temperature of the heat used. Alkali metal and alkaline earth metal chlorides have many advantages, such as relatively high melting point and latent heat, stable performance and low cost. At present, many kinds of chloride salts have been chosen as PCM at moderate-high temperatures[14,15]. In addition, the chloride salt and fluoride salt also have been chosen as two candidate materials for cooling heat transfer medium in the next generation nuclear power plant by Oak Ridge National Laboratory[16,17]. The melting point of the molten eutectic chloride of sodium chloride and magnesium chloride (NaCl-52 wt% $MgCl_2$) is 445 °C. Compared with other kinds of chloride salts, the mixture salt has the advantages of higher fusion latent heat (430 J/g) and lower cost, which has good development potential as a PCM at moderate-high temperatures[18]. But the

Received date: February 18, 2019
Foundation item: National Natural Science Foundation of China (51441003); Qinghai Natural Science Foundation (2016-ZJ-759)
Corresponding author: Jia Hongguang, Professor, Qinghai University, Xining 810016, P. R. China, Tel: 0086-971-5310440, E-mail: hgjia@hqu.edu.cn

molten chloride salt is strongly corrosive to metal container and pipes. Consequently, it is necessary to investigate the corrosion behavior of common metals in the molten eutectic chloride.

Shores et al[19] have demonstrated by theoretical calculations and experimental studies that the corrosion rate of Fe-Cr-Ni alloy in molten sodium sulfate (Na_2SO_4) increases by about 100 times after adding sodium chloride (NaCl). Consequently, the sodium chloride acts as a catalyst in the corrosion process of the Fe-Cr-Ni alloys in molten sodium sulfate (Na_2SO_4) with the sodium chloride (NaCl)[20-22]. Besides, thermal diffusion coatings of chromic oxide (Cr_2O_3) and aluminum oxide (Al_2O_3) were prepared on the Inconel 625 (NiCr alloy) surface by Ma et al[23]. Then the corrosion behaviors of the two kinds of coatings in molten potassium chloride-magnesium chloride (KCl-$MgCl_2$), sodium chloride-calcium chloride (NaCl-$CaCl_2$) and potassium chloride-calcium chloride (KCl-$CaCl_2$) were studied at 900 °C. Results show that the chromic oxide (Cr_2O_3) coating has poor corrosion resistance than aluminum oxide (Al_2O_3) for high solubility of the chromic oxide (Cr_2O_3) in molten chloride salt. The corrosion behaviors of 321 stainless steel in molten barium chloride-calcium chloride ($BaCl_2$-$CaCl_2$) at 950 °C were studied by Amin N.[24]. The alloy is corroded seriously because of volatile material with chromium formed. The corrosion resistance of the alloy in the molten chloride is declined for the alloying element chromium[25]. Therefore, Otero E.[26] studied the corrosion behavior of a low chromium steel (12CrMoV) in molten eutectic salt of lead chloride-potassium chloride (PbCl-KCl). The alloy is corroded obeying a linear law. An effective protective film does not form on the specimen surface. In addition, it was also concluded that carbon plays an important role in the corrosion process. Electrochemical behaviors of SS310, SS347, In800H and IN625 (SS310 and SS347 are stainless steel, In800H is NiFeCr alloy, IN625 is NiCr alloy) in melting sodium chloride-lithium chloride (NaCl-65.58 wt% LiCl) at 650~700 °C were studied by Gomez-Vidal[27]. The corrosion resistance increases with increasing the content of nickel. In the four kinds of alloys, the lowest corrosion rate is 2.80±0.38 mm/a (IN625) in the molten salt at 650 °C. The lowest corrosion rate is much higher than the standard corrosion rate (50 μm/a). Therefore, the alloy cannot meet the requirements of materials as chloride heat storage containers[27].

The research team of this paper has found that a magnesium oxide (MgO) shell is formed on the specimen surface when metal is corroded in the molten eutectic chloride of sodium and magnesium (NaCl-52 wt% $MgCl_2$), which severely affects the corrosion behavior[28,29]. Therefore, the corrosion behavior of three kinds of model Fe-Cr-Ni alloys in molten eutectic NaCl-$MgCl_2$ was discussed, especially the formation mechanism of the magnesium oxide (MgO) and its influence on the corrosion behavior. A high-carbon steel was also studied as a compared specimen. Because of high moisture-absorb of the magnesium chloride ($MgCl_2$), which is inevitable in engineering applications, the corrosion experiments were carried out under air atmosphere. This study is the foundation of selecting the best container material for storing molten chloride, and the development of an advanced material which is corrosion-resistant in a molten chlorinated salt.

1 Experiment

For the three kinds of model Fe-Cr-Ni alloys, reference to ASTM A240/A 240M-05, based on the main composition of stainless steels 201, 304 and 321, taking electrolytic pure iron, chromium, nickel and titanium as raw materials, three kinds of model Fe-Cr-Ni alloy were melted in medium frequency induction melting furnace (type: SP-25TC) under argon atmosphere. Trace elements of carbon, sulphur, phosphorus, silicon and manganese were ignored. The nominal (Nom.) and detected (Det.) compositions of the three kinds of alloys are showed in Table 1. A commercially available steel T8 was used as the carbon steel specimen. The four kinds of alloys were marked as 1#, 2#, 3# and 4#. All specimens were cut into rectangles with the size of 10 mm×10 mm×3 mm, and then polished by 600#, 1200# and 2000# silicon carbide (SiC) papers, successively. After cleaning and drying, all specimens were stored in a drying vessel. The compositions of specimens were detected by the X-ray spectroscopy (XRF, ZSX Primus α), as shown in Table 1.

Magnesium chloride (registered trademark: Aladdin, purity≥99 wt%) and dried sodium chloride (registered trademark: Shuangshuang, purity≥99.5 wt%) were weighted by an electronic balance with a precision of 0.1 mg (SOPTOP-FA2004, Shanghai Sunny Hengping Scientific Instrument Co., Ltd.). After the two kinds of salts were mixed well in four corundum crucibles, they were put in a muffle furnace which was heated to 520 °C. After the mixture salt was melted completely, four specimens of each kind of alloys were completely immersed in the molten salt in one crucible. Before all alloys were immersed in, they were coated due to the thermal stress. The surface area and mass of specimens were measured and weighted by a vernier caliper (Hengliang-530-150, accuracy 0.02 mm, Shanghai Hengliang Measuring Tool Co., Ltd.) and the electronic balance (SOPTOP-FA2004), respectively. After corrosion for 10 h, all specimens were taken out from the muffle furnace

Table 1 Nominal and detected composition of four kinds of alloys (wt%)

Specimen	Cr		Ni		Ti		C	Fe
	Nom.	Det.	Nom.	Det.	Nom.	Det.	Nom.	Det.
Carbon steel, 1#	–	–	–	–	–	–	0.8	Bal.
201, 2#	14.5	14.7	4.5	4.3	–	–	–	Bal.
304, 3#	18.0	18.0	9.5	9.6	–	–	–	Bal.
321, 4#	18.0	19.6	4.5	5.4	1. 0	0.8	–	Bal.

and cooled to room temperature. One specimen was treated by the submerged-water method. The submerged-water method is that a specimen is soaked in distilled water silently at room temperature. After the residual salt on specimen surface was completely dissolved, the specimen was soaked in alcohol and then dried by cold air. The corrosion products on the specimen surface were protected carefully during the process. The remaining three specimens were treated by the mechanical treatment in accordance with GB/T 16545-1996 requirements, that is, specimens are cleaned in distilled water and alcohol by ultrasonic cleaning machine for 10 and 5 min, and then dried by cold air. Then those specimens were weighted by the electronic balance (SOPTOP-FA2004). Their mass changes were calculated. After that, all specimens were immersed in a fresh molten salt for the second time corrosion experiments. The above procedure was repeated for 8 times.

After the last corrosion (after corrosion for 80 h), for each alloy, the specimens was treated by the submerged-water method too. The cross section of the second specimen was polished without water[29]. The morphology and element distribution on the corroded specimen surface and cross section were analyzed by scanning electron microscope (SEM) and energy dispersive X-ray detector (EDS) (ZEISS MERLIN Compact and JSM-6610LV). For the third specimen, corrosion products on the specimen surface were analyzed by the X-ray diffractometer (XRD, Rigaku D/max-2500/PC, Copper Kα radiation source, λ=0.1541 nm) after the residual salt was cleared by the submerged-water method.

2 Results and Discussion

2.1 Experimental result

After the corrosion products on specimens were cleared as thorough as possible by the mechanical treatment, the relationship of the cumulative mass change per unit surface of the four kinds of specimens Δm_i (i is specimen number, i=1, 2, 3, 4) and corrosion time t is shown in Fig.1. It is found that after corrosion for 10 h, the mass of the carbon steel specimen (1#) increases approximately by obeying a line law. However, the mass of other three kinds of model Fe-Cr-Ni alloys tends to decrease linearly. The fitting formulas are as follows:

$$\Delta m_1=0.0027t+0.0068 \quad (1)$$

$$\Delta m_2=-0.0102t+0.3691 \quad (2)$$

$$\Delta m_3=-0.0473t+0.6188 \quad (3)$$

$$\Delta m_4=-0.0296t+0.5575 \quad (4)$$

During the corrosion from 10 h to 70 h, as described above, after the corrosion products on specimen surface were also cleared as thorough as possible by the mechanical treatment, the average mass changes of the four kinds of specimens per unit time Δm_{vi} ($mg\cdot cm^{-2}\cdot h^{-1}$) are shown in Fig.2. The mass of the specimen 1# increases by 0.013±0.08 $mg\cdot cm^{-2}\cdot h^{-1}$. The mass of 2#, 3# and 4# specimens decreases by 0.017±0.08, 0.041±0.08 and 0.039±0.08 $mg\cdot cm^{-2}\cdot h^{-1}$, respectively. According to the analysis later, only a few corrosion products adhere to the three kinds of model Fe-Cr-Ni alloy surface. So, when the products are neglected, the corrosion rate of 2#, 3# and 4# specimen is 70.2, 178.13 and 162.6 μm/a, respectively.

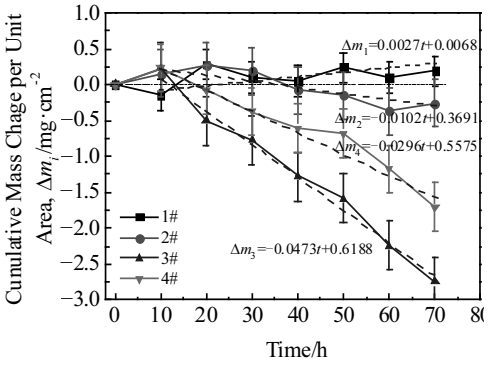

Fig.1 Relationships between the cumulative mass change and exposure time

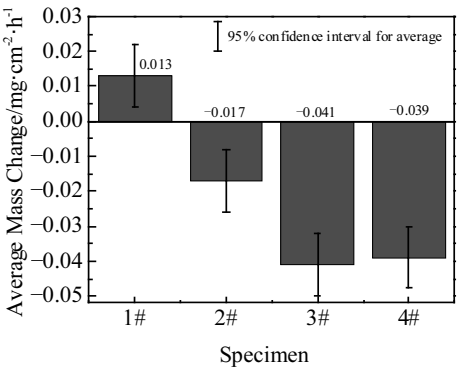

Fig.2 Average mass change of four kinds of specimens per unit time during corrosion from 10 h to 70 h

After corrosion for 10 and 80 h, the XRD results of the four specimens' surface treated by the submerged-water method are showed in Fig.3. As shown in Fig.3a, only iron and magnesium oxide (MgO) are detected on the carbon steel specimen surface. It is found from Fig.3b~3d that a certain amount of magnesium oxide (MgO) and compound phases of Fe-Ni ($FeNi_3$ and $Fe_{0.64}Ni_{0.36}$) are found on the three kinds of model Fe-Cr-Ni alloys. Another kind of compound phase of Fe-Cr-Ni ($Cr_{0.19}Fe_{0.7}Ni_{0.11}$) is found on the surfaces of specimens 304 and 321. Trace mixed oxide of nickel and magnesium is also detected on the surfaces of specimens 304 and 321. After corrosion for 80 h, the relative content of magnesium oxide (MgO) in the four kinds of specimens is obviously higher than after corrosion for 10 h.

After corrosion for 10 h and treated by the submerged-water method, the surface morphology and EDS spectra of the four kinds of specimens are shown in Fig.4. The unlabeled peak is gold (Au).

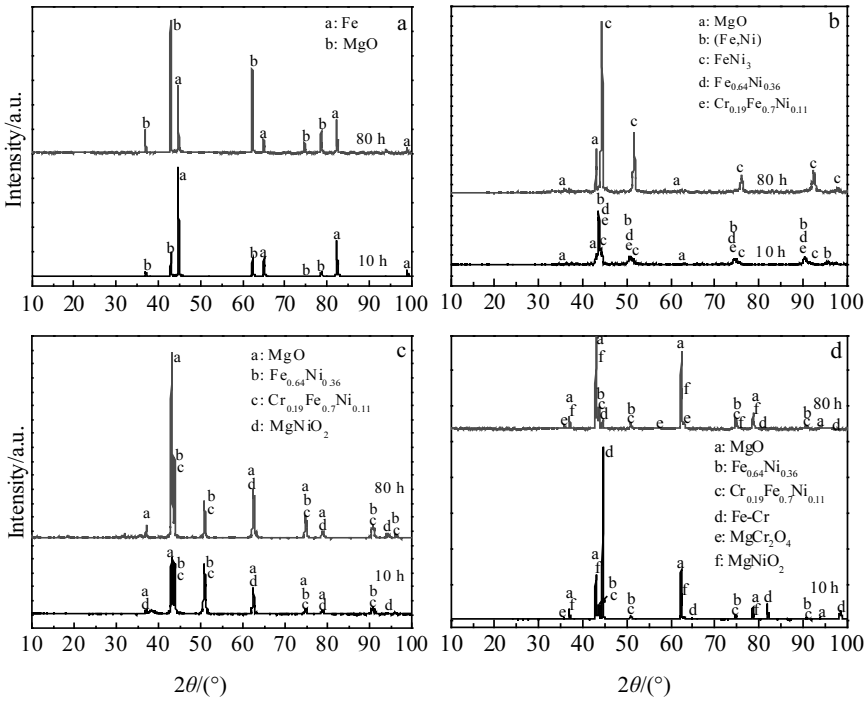

Fig.3 XRD patterns of four specimen surfaces after exposure for 10 and 80 h: (a) 1#, (b) 2#, (c) 3#, and (d) 4#

As shown in Fig.4a and Fig.4b, specimen 1# surface is covered by a thick and dense shell. The contents of magnesium and oxygen elements (location 2) on the shell are higher. Combined with the XRD results in Fig.3a, the main composition of the shell is magnesium oxide (MgO). After the magnesium oxide shells are exfoliated locally, the specimen substrate is exposed (location 1, iron is the major elements). A few irregularly particles rich in magnesium oxide (MgO) are attached to the magnesium oxide shell (location 3).

For the three kinds of model Fe-Cr-Ni alloys, after corrosion for 10 h, thin shells or particles with high content of Mg and O elements are formed on the surface too. Combined with the XRD results in Fig.3b~3d, MgO shells or particles also form on the surface of three kinds of specimens, as shown in location 2 in Fig.4c, 4e and 4g. However, the MgO shell peels off more seriously than on the carbon steel surface, as shown in Fig.4a.

After corrosion for 80 h and submerged-water method treatment, surface morphology and EDS results of the carbon steel, 201, 304 and 321 model Fe-Cr-Ni alloy specimens are shown in Fig.5. The unlabeled peak is Au too. Combined with XRD results in Fig.3, the surface of the carbon steel specimen is also covered by a magnesium oxide shell, as shown in Fig.5a. And many angular magnesium oxide particles adhered to the shell are larger than those a in Fig.4a, which is because the Mg^{2+} is oxidized and then deposited in the molten salt. This process will be discussed in detail later.

Compared with the surface morphology after corrosion for 10 h shown in Fig.4, it is found from Fig.5c, 5e and 5g that all the surface of three kinds of model Fe-Cr-Ni alloys are loose. Except for the MgO shells or particles, their surfaces are skeletal microstructure. Combined with XRD results in Fig.3, the main phases on the surface of three kinds of model Fe-Cr-Ni alloys are compound phases of Fe-Ni ($FeNi_3$ and $Fe_{0.64}Ni_{0.36}$). A few compound phases of Fe-Cr-Ni ($Cr_{0.19}Fe_{0.7}Ni_{0.11}$) and the oxide of chromium, nickel and magnesium are also detected on the surface of 304 and 321 specimen with higher content of iron and nickel.

After corrosion for 80 h, the EDS results of the cross section of 1#, 2#, 3# and 4# specimens are shown in Fig.6a~6d, respectively. There is a non-conductive shell on the surface of specimen 1#, and the content of oxygen and magnesium in the shell is higher than that in matrix. Combined with previous results (Fig.3a, Fig.5a and 5b), the shell is magnesium oxide (MgO). A slight corrosion along the grain boundary can also be found.

As shown in Fig.6b, a corrosion shell about 20 μm is formed near the surface of the specimen 2#. On the corrosion layer, the microstructure is slightly loose, and the contents of iron and chromium decrease, but the content of nickel increases slightly. Near the corrosion layer surface, the contents of magnesium and oxygen increase slightly, and other elements do not change obviously. Combined with the XRD results in Fig.3b and surface morphology in Fig.5c and 5d, a few MgO particles adhere to the skeletal specimen surface.

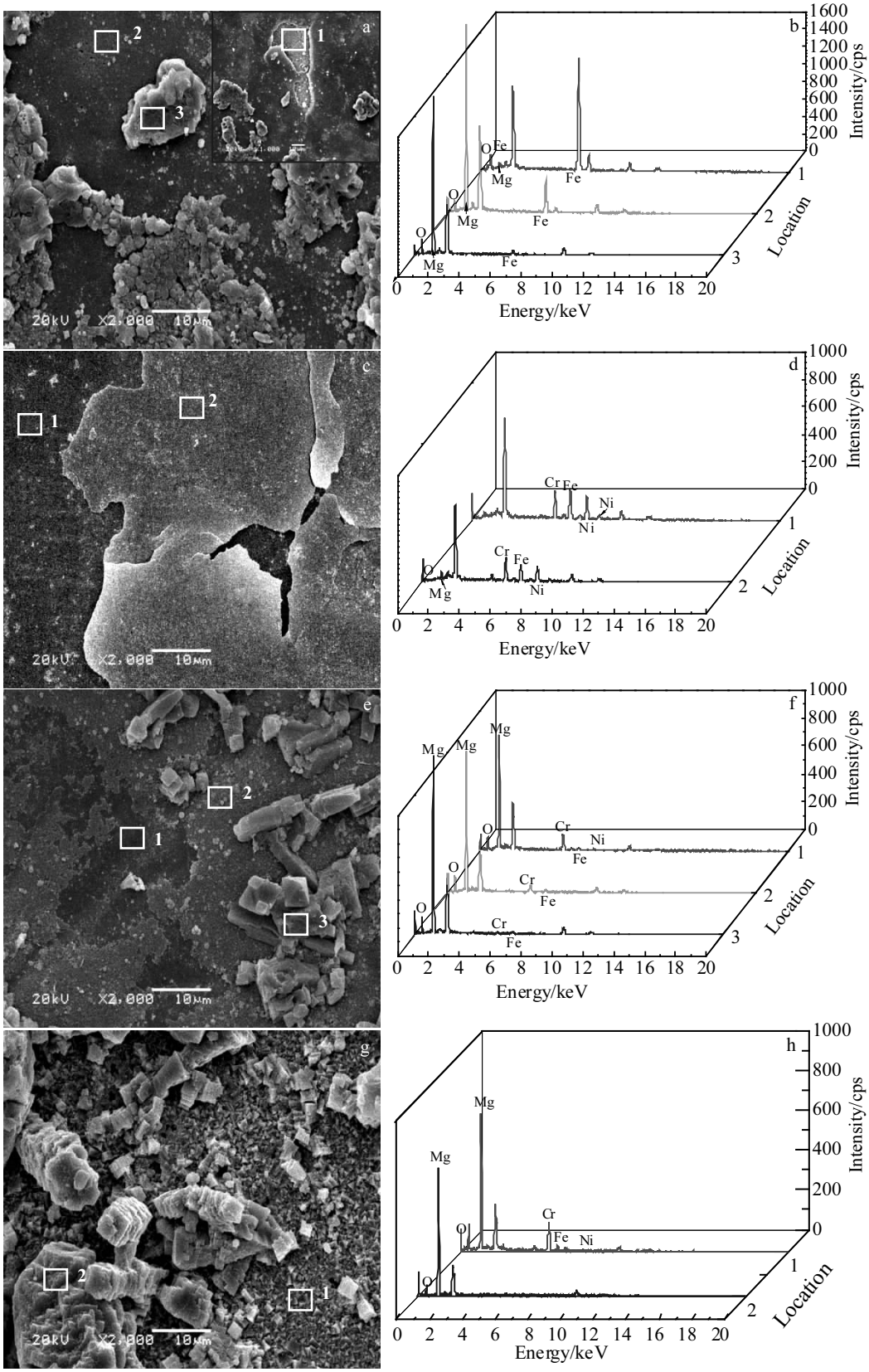

Fig.4 Surface morphologies (a, c, e, g) and local EDS spectra (b, d, f, h) of the four kinds of specimens after corrosion for 10 h and treated by the submerged-water method: (a, b) 1#, (c, d) 2#, (e, f) 3#, and (g, h) 4#

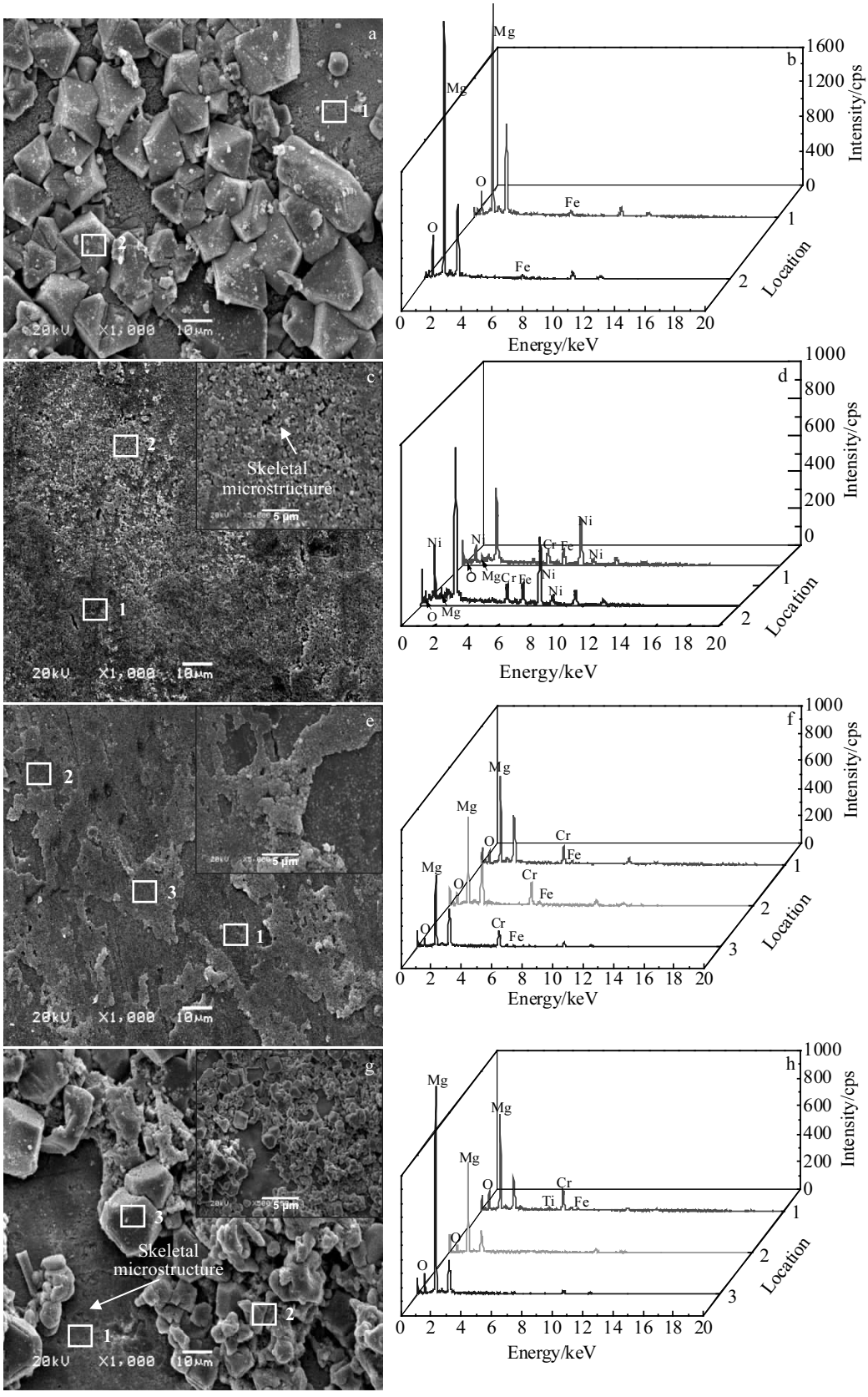

Fig.5 Surface morphologies (a, c, e, g) and local EDS spectra (b, d, f, h) of four kinds of specimens after corrosion for 80 h and treated by the submerged-water method: (a, b) 1#, (c, d) 2#, (e, f) 3#, and (g, h) 4#

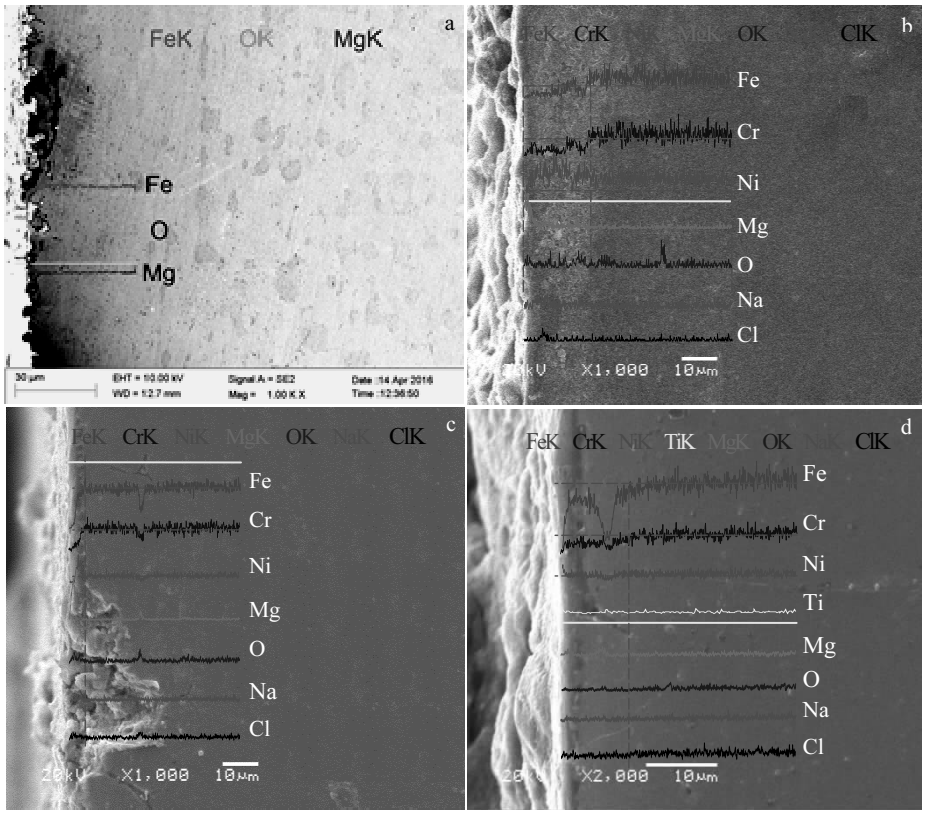

Fig.6 EDS results of the cross section of four kinds of specimens after corrosion for 80 h: (a) 1#, (b) 2#, (c) 3#, and (d) 4#

In Fig.6c, a large corrosion pit is found on the cross section of specimen 3#. In addition, a loose corrosion layer about 5 μm is formed near the surface. In the corrosion layer, the contents of iron and chromium also decrease obviously, while the contents of nickel, magnesium and oxygen increase slightly.

As shown in Fig.6d, in the range of 15 μm on the specimen 4# surface layer, the content of chromium is also lower than that in the specimen matrix, and corrosion cracking exists in local position. In the crack, except for the decrease of iron content, the content of magnesium and oxygen increases slightly, which indicates that the Mg^{2+} penetrates into the specimen matrix and corrosion crack is also oxidized. Any results related to alloy element titanium were not found in this experiment. Carbon and its compound are also not found obviously from the results of XRD in Fig.3 and EDS in Fig.5 too.

2.2 Discussion

The molten eutectic chloride of the sodium and magnesium (NaCl-52 wt% $MgCl_2$) is a strong electrolyte, in which alloy will be corroded in electrochemical reactions. The metal atom in the specimen with low potential is an anode. The cathode is oxygen atoms that are dissolved in the molten salt from the air atmosphere. For specimen 1#, reactions occur as follows[29]:

$$Fe \rightarrow Fe^{2+}+2e \quad (5)$$

$$O+2e \rightarrow O^{2-} \quad (6)$$

$$O^{2-}+Mg^{2+} \rightarrow MgO \quad (7)$$

The magnesium oxide shell deposits on the specimen surface, as shown in Fig.4a, Fig.5a and Fig.6a. The mass of the specimen decreases according to Eq.(5). In addition, because of the low oxygen partial pressure in molten chloride salt, it is found from XRD results in Fig.3a that the oxides of iron cannot be detected obviously after corrosion for 10 h. Therefore, the oxidation reaction of iron and its oxide deposited on the specimen surface are neglected. Consequently, the mass increase of specimen 1# is the results of reaction in Eq.(7).

If only the reactions of Eq.(5~7) occur for the 1# specimen, it can be assumed as follows:

1) After the reaction of Eq.(5), the lost electrons are completely absorbed by the solute oxygen in the molten salt and then reaction of Eq.(6) occurs.

2) The formed magnesium oxide (MgO) in the reaction of Eq.(7) deposits on the specimen surface completely.

Based on the electron conservation law, the specimen mass is reduced by 28.6% after reaction of Eq.(5~7). However, as shown in Fig.1, the mass of specimen 1# does not decrease, but increases with corrosion time. The experimental results are inconsistent with the above analysis, which indicates that

other reactions occur on the surface of 1# specimen in addition to the reactions of Eq.(5~7). The following reaction may occur:

$$Fe \rightarrow Fe^{3+}+3e \quad (8)$$

Ferrous ion (Fe^{2+}) and ferric ion (Fe^{3+}) will react with Cl^- in the molten salt, and then escape from the corrosion system in the form of iron dichloride ($FeCl_2$) or ferric trichloride ($FeCl_3$). Because the "T_4 temperature" of iron dichloride ($FeCl_2$) or ferric trichloride ($FeCl_3$) is 527 and 165 °C, respectively, which are below or close to the test temperature here[30]. The magnesium oxide (MgO) will deposit on the specimen surface. Based on the above two assumptions and reactions of Eq.(6~8), the specimen mass will increase by 7.1%, which is consistent with mass change results of specimen 1# in Fig.1.

In addition, because of the high moisture-absorb of the magnesium chloride ($MgCl_2$), a magnesium chloride hexahydrate ($MgCl_2 \cdot 6H_2O$) will form after the magnesium chloride ($MgCl_2$) absorbs moisture during heating and melting process. The magnesium chloride hexahydrate ($MgCl_2 \cdot 6H_2O$) will decompose into magnesium oxide (MgO) at the test temperature. Then the magnesium oxide particle deposits on specimen surface too, where heterogeneous nucleation substrate is located, and grows up continuously. At last, the magnesium oxide particles will grow up to a continuous and compact magnesium oxide shell on the specimen surface. A part of magnesium oxide particles attached on the shell also grows up with the extension of exposure time, as shown in Fig.4a and Fig.5a.

As shown in Fig.5a, 5b and Fig.6a, after corrosion for 80 h, the magnesium oxide shell on the T8 specimen surface is very thick, compact and large. In addition, because of high energy at grain boundary, it is corroded preferentially. The magnesium oxide (MgO) inserts into sample matrix along the grain boundary, which will increase connection strength between the magnesium oxide shell and matrix. Furthermore, as shown in Fig.1 and Fig.2, although all the specimens were cleared by the ultrasonic cleaning machine in distilled water and alcohol after corrosion in the molten salt, the mass of the 1# specimen still increases. Based on the above analyses, it is thought that the bonding force between the dense magnesium oxide shell and the specimen surface is sufficiently strong to protect the specimen from corrosion in the molten salt. The corrosion process schematic diagram of the T8 steel is shown in Fig.7a. Consequently, the carbon steel can be listed as a vessel and pipe candidate material.

As shown in Fig.1, the masses of the three kinds of model Fe-Cr-Ni alloys (201, 304 and 321) decrease continuously with the extension of exposure time. It is also found from Fig.4a~4c that after corrosion for 10 h, a thin magnesium oxide shell is formed on those specimen surfaces, but it is very loose and incomplete. The specimen substrate is exposed locally. After corrosion for 80 h, the three kinds of Fe-Cr-Ni alloys are different from specimen 1#. Their surfaces are looser, flaking, exposing looseness. As shown in Fig.5b~5d, a porous matrix (skeletal microstructure) instead of a thick and compact magnesium oxide shell appears on the carbon steel specimen. It is reported in Ref.[31] that the corrosion potential of Ni based alloy in molten chloride salt decreases with increasing the content of alloying element Cr. Consequently, it is thought that the chromium is preferentially corroded like the reaction in Eq.(5) near the Fe based specimen surface too. Then the chromium ion (Cr^{3+}) is volatilized in the form of chromic chloride ($CrCl_3$) because of low T4 temperature (531 °C)[30]. Those reactions are as follows:

$$Cr \rightarrow Cr^{3+}+3e \quad (9)$$

$$Cr^{3+}+ Cl^- \rightarrow CrCl_3\ (g) \quad (10)$$

With the extension of the exposure time, the microstructure of the specimen surface gradually becomes loose. And the content of chromium decreases near the specimen surface, as shown in Fig.6b~6d. The content of nickel increases slightly accordingly. The compound phases which are rich in nickel and iron are formed ($FeNi_3$ or $Fe_{0.64}Ni_{0.36}$).

Although a plenty of magnesium oxide (MgO) is formed on the 201, 304 and 321 specimen surfaces, as shown in Fig.3 and Fig.5, the magnesium oxide particles adhered to the loose specimen surfaces will peel off, forming the skeletal microstructure. Then the molten salt permeates into the specimen matrix along the corrosion gap. As shown in Fig.1, the mass of all three kinds of model Fe-Cr-Ni alloys decreases linearly. The corrosion process is shown in Fig.7b.

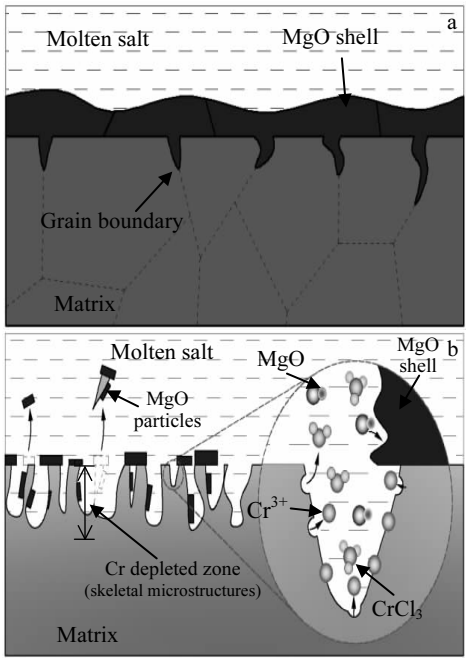

Fig.7 Corrosion process schematic diagrams of carbon steel (a) and three kinds of model Fe-Cr-Ni alloys (b) in molten NaCl-$MgCl_2$

Consequently, because the chromium dissolves preferentially, as shown in Fig.1, the mass loss of the specimen 201 with low content of chromium is less than that of the specimens 304 and 321. The phase with chromium (such as the compound phases of $Cr_{0.19}Fe_{0.7}Ni_{0.11}$ on the surface of 304 and 321 specimens) is not found obviously on the 201 specimen surface after corrosion for 80 h, as shown in Fig.3. The specimens 304 and 321 have similar chromium content and different nickel, but the mass loss of them are similar. So the alloy element chromium is a key factor in affecting the corrosion behavior of three kinds of model Fe-Cr-Ni alloys in the molten chloride salt.

The skeletal microstructure with large surface area is rich in nickel. As shown in Fig.3, trace of mixed oxide of nickel and magnesium is also detected on the model Fe-Cr-Ni alloy surface.

3 Conclusions

1) The mass of the carbon steel increases. Because of the decompose of magnesium chloride hexahydrate ($MgCl_2·6H_2O$) and the reaction between magnesium ion (Mg^{2+}) and oxygen ion (O^{2-}), a dense and relatively complete magnesium oxide shell is formed on the carbon steel surface. The magnesium oxide shell can insert into the sample matrix along the corroded grain boundary, which increases bonding force between the magnesium oxide shell and the specimen matrix, and protects the specimen from corrosion in the molten salt.

2) Surfaces of three kinds of model Fe-Cr-Ni alloys are loose and porous after corrosion in the molten salt. Their masses decrease continuously with the extension of exposure time. Because the chromium dissolves preferentially as a anode, magnesium oxide shells and particles on the skeletal microstructure cannot protect the specimen matrix.

3) Compared with the alloying element nickel in three kinds of Fe-Cr-Ni alloys, the key factor affecting corrosion of those model Fe-Cr-Ni alloys in the molten chloride salt is the content of chromium.

4) The three kinds of Fe-Cr-Ni alloys cannot be used as a container or pipe for the molten chloride salt as PCM. The corrosion resistance of the carbon steel is better than that of Fe-Cr-Ni alloys.

References

1 Liu G L, Wang H, Yuan X Z *et al*. *Applied Thermal Engineering*[J], 2019, 156(25): 14

2 Lehtola Timo, Zahedi Ahmad. *Sustainable Energy Technologies and Assessments*[J], 2019, 35: 25

3 Chen Y L, Wang L J, Wang W Z *et al. Applied Catalysis B-Environmental*[J], 2017, 209: 110

4 Chou C S, Huang Y H, Wu P. *Applied Energy*[J], 2014, 118: 12

5 Asgharian H, Baniasadi E. *Journal of Energy Storage*[J], 2019, 21: 186

6 Zhang J J, Wang H, Yuan X Z *et al. Journal of Photochemistry and Photobiology C: Photochemistry Reviews*[J], 2019, 38: 1

7 Cao M S, Wang X X, Zhang M *et al*. *Advance Functional Materials*[J], 2019, 29(25): 1 807 398

8 Cao M S, Wang X X, Cao X Q *et al*. *Small*[J], 2018, 14(29): 18 009 871

9 Tayyab R S, Hafiz M A. *Solar Energy*[J], 2019, 183: 173

10 Choi Y J, Mae M, Kim H B. *Solar Energy*[J], 2019, 186: 277

11 Mohamad A, Mehdi G, Alibakhsh K *et al*. *Renewable Energy*[J], 2019, 140: 419

12 Zhang P, Ma F, Xiao X. *Applied Energy*[J], 2016, 173: 255

13 García-Martín G, Lasanta M I, Encinas-Sánchez V *et al. Solar Energy Materials and Solar Cells*[J], 2017, 161: 226

14 Li Y Y, Xu X K, Wang X X *et al. Solar Energy*[J], 2017, 152: 57

15 Vignarooban K, Xu X H, Arvay A *et al. Applied Energy*[J], 2015,146: 383

16 Williams D F. *Assessment of Candidate Molten Salt Coolants for the NGNP/NHI Heat-transfer Loop*[D]. Washington: Oak Ridge National Laboratory, 2006

17 Gomez-Vidal J C, Fernandez A G, Tirawat R *et al. Solar Energy Materials and Solar Cells*[J], 2017, 166: 234

18 Kenisarin M M. *Renewable Sustainable Energy Reviews*[J], 2010, 14(3): 955

19 Shores D A, Mohanty B P. *Corrosion Science*[J], 2004, 46(12): 2909

20 Li Y S, Spiegel M, Shimada S. *Materials Letters*[J], 2004, 58(29): 3787

21 Shinata Y, Nishi Y. *Oxidation of Metals*[J], 1986, 26: 201

22 Shinata Y. *Oxidation of Metals*[J], 1987, 27(5-6): 315

23 Ma H F, Zhu M, Zhu Q *et al*. *Materials Science Forum*[J], 2014, 809-810: 589

24 Amin N, Amin M M, Jamaludin S B *et al. Materials and Technologies*[J], 2008, 42(6): 273

25 Li Y S, Niu Y, Spiegel M. *Corrosion Science*[J], 2007, 49(4): 1799

26 Otero E, Pardo A, Pérez F J *et al. Oxidations of Metals*[J], 1998, 49: 467

27 Gomez-Vidal J C, Tirawat R. *Solar Energy Materials and Solar Cells*[J], 2016, 157: 234

28 Wang J W, Zhang C Z, Li Z H *et al. Solar Energy Materials and Solar Cells*[J], 2017,164: 146

29 Wang J W, Zhou H X, Zhong R J *et al. Rare Metal Materials and Engineering*[J], 2017, 46: 935

30 Bender R, Schütze M. *Materials and Corrosion*[J], 2003, 54: 567

31 Gomez-Vidal J C, Fernandez A G, Tirawat R *et al*. *Solar Energy Materials and Solar Cells*[J], 2017, 166: 222

碳钢和铁-铬-镍基合金在相变储能材料用熔融共晶氯化钠和氯化镁中的腐蚀行为

王军伟[1,2]，鲍泽龙[1]，叶海花[1]，马　清[3]，贾红光[1,2]

(1. 青海大学 机械工程学院，青海 西宁 810016)

(2 青海大学 青海省新型轻合金重点实验室，青海 西宁 810016)

(3. 青海大学 高原生态与农业国家重点实验室，青海 西宁 810016)

摘　要：研究了 3 种铁-铬-镍基合金（Fe-Cr-Ni）和一种碳钢试样在 520 ℃熔融共晶 NaCl-$MgCl_2$ 盐中的腐蚀行为。结果表明，碳钢试样晶界处 Fe 原子优先变为亚铁离子（Fe^{2+}）和铁离子（Fe^{3+}），发生了严重的沿晶腐蚀，但表面形成了厚而致密的 MgO 壳，对试样起到了一定的保护作用。3 种 Fe-Cr-Ni 基试样表面也形成了 MgO 壳，但因铬元素优先被腐蚀，试样表面形成了疏松的富 Ni 骨架状微观组织结构，MgO 壳或颗粒极易剥落，未能起到有效的保护作用；Cr 含量越高，腐蚀越严重。对于太阳能储能技术，在廉价的铁基合金中添加镍元素作为熔融氯化盐相变储热介质的容器或者管道材料，具有良好发展前景。

关键词：熔融氯化盐；高温腐蚀；氧化镁；不锈钢；碳钢

作者简介：王军伟，男，1986 年生，博士，教授，青海大学机械工程学院，青海 西宁 810016，电话：0971-5310440，E-mail: wangjw86@163.com